Multi-scale Modeling and Simulation of a Novel Membrane Reactor (MR)/Adsorptive Reactor (AR) Process

Seçgin Karagöz
Dept. of Chemical and Biomolecular Engineering,
University of California, Los Angeles, Los Angeles, CA, 90095
Theodore T. Tsotsis
Mork Family Department of Chemical Engineering & Materials Science,
University of Southern California, Los Angeles, Los Angeles, CA, 90089
Vasilios I. Manousiouthakis (corresponding author)
Dept. of Chemical and Biomolecular Engineering,
University of California, Los Angeles, Los Angeles, CA, 90095

Abstract

The objective of this study is the modeling and simulation of a novel process, consisting of a membrane reactor (MR)/adsorptive reactor (AR) sequence that intensifies equilibrium-limited reactions and associated separation processes. A comprehensive, multi-scale, multiphase, steady-state/dynamic, computational fluid dynamics (CFD)-based process model is developed, that quantifies the many underlying complex physicochemical phenomena occurring at the pellet, and reactor scales. Model simulations are then carried-out, to study the influence of the individual units' operating and design parameters on overall system performance, and to better understand this simultaneous reaction/separation, steady-state/cyclic process. Simulation-based optimization studies are then carried out to identify acceptable ranges for both operating and design parameters, so as to meet pre-defined process performance specifications.

1. Introduction

Procurement of energy at environmentally-friendly and economical levels is both a great challenge and an opportunity for the world. To this end, the use of CO_2 capture/sequestration systems is currently being considered during the development of new technologies, as well as in the improvement of existing technologies for power generation [1]. One such example is the application of carbon capture technologies to the Integrated Gasification Combined Cycle (IGCC) process [2]. The IGCC process integrated with carbon capture generates electricity from a solid or liquid fuel, by (1) converting the fuel into syngas (a mixture of CO, CO_2, H_2, H_2O, CH_4) at high pressures, (2) cleaning-up the produced syngas from problematic impurities (e.g., COS, H_2S, HCl, Hg, etc.), (3) converting the remaining CO into CO_2 by utilizing a sequence of reactors where the Water Gas Shift Reaction (WGSR) takes place, (4) separating the H_2 and CO_2 out of the resulting mixture, (5) generating electricity in a combined-cycle power block consisting of a gas turbine and a steam turbine, (6) and drying and compressing the CO_2 for sequestration purposes.

Process intensification (PI) encompasses any chemical engineering development offering drastic process technology improvements, in regard to a variety of metrics. Such intensification has the potential to improve process efficiency and economics. As part of the intensification procedure, integration of multiple operations (e.g., reaction and separation) in a single unit is used as a robust tool to improve the existing process' efficiency, and to reduce energy consumption, and unwanted outputs/by-products [3-4]. Adsorption, absorption and membrane-based separations are some of the techniques available to accomplish such intensification for the IGCC process, as part of a multifunctional separation/reactor system for simultaneous production, separation, and purification of hydrogen from the syngas mixtures [5-6]. In particular, in this study we consider the combined use of adsorptive reactor (AR) and membrane reactor (MR) technologies for the efficient production and recovery of the produced gases from the gasifier off-gas. Via the combined use of these reactors, the reaction products (e.g. H_2, CO_2) are selectively removed by the adsorbent (in the AR) and the membrane (in the MR), so that the equilibrium conversion is shifted in both reactors toward the product side, and H_2 and CO_2 product separation is also accomplished. The employed AR and MR technologies also present some other promising features, including lower reaction operating temperatures, reduced material costs, and increased operation safety. Moreover, employing this efficient MR and AR system eliminates the need for using excess steam in the reaction, minimizes the downstream purification requirements, and reduces the amount of catalyst needed for attaining the desired conversion level [7-8].

The main focus of this study is to demonstrate a novel membrane/adsorption-enhanced IGCC process, which utilizes a novel membrane reactor (MR)/adsorptive reactor (AR) sequence. The integration of these two reactive separation technologies creates a synergy that significantly increases overall process efficiency and results in higher reaction rates, yields and selectivity [7-8] when compared to the individual MR [9-25] and AR [26-33] processes which separate only one of the reaction products (e.g. H_2 or CO_2).

The study of multiphase transport/reaction phenomena is, of course, of interest to a wide range of separation and reactor applications [34-36] involving simultaneous heat, momentum, and multi-component mass transport [37-39]. A marked characteristic of such multiphase reactor/separator systems is the need to explicitly account for the reaction/transport processes within the porous catalysts/adsorbents/membranes themselves. For the MR/AR process studied here, accounting for all these phenomena dictates the use of so-called heterogeneous models rather than simplified pseudo-homogeneous models that have, to date, dominated the modeling literature. The most crucial advantage of using such models in the modeling of reactors and separators, is their ability to solve the transport/reaction equations separately for each phase (bulk reactor, catalyst, adsorbent, and membrane), explicitly accounting for gradients inside each phase and in between phases, and thus providing satisfactory modeling results for large-scale, commercial units where such intra-particle gradients may have a substantial impact. Thus, these multi-scale models are not only adequate for the lab-scale reactors/separators where one utilizes powdered catalysts/adsorbents, but also for the commercial-scale systems which employ larger size pellets to avoid large pressure drops, particularly under the high-pressure conditions of the IGCC application.

The objective of this work, therefore, is to first develop multi-scale MR/AR models, which describe in detail the species/energy transport phenomena within the porous catalyst/adsorbent pellets, and their dependence on the pellet's location along the reactor's length, together with the species/energy transport phenomena in the reactor's bulk phase. Subsequently, employing these models we aim to demonstrate the intensification attained by the proposed integrated MR/AR process, through elimination of the need for use of complex and costly downstream unit operations, such as e.g., the two-stage Selexol process.

In order to accomplish the aforementioned objective, we first focus on the design of each individual unit prior to the optimization of the overall process. We employ the comprehensive, multi-scale, multiphase, CFD models developed to quantify the complex physicochemical phenomena occurring in each unit, with the aim to provide the basis to better understand, and to intensify the integrated reaction/separation, steady-state/cyclic process. We then carry-out simulations in order to study the influence of the individual units' operating and design parameters. For the MR component, for example, we investigate the effect of temperature, pressure, W_{cat}/F_{CO} ratio, inlet H_2O/CO molar ratio, permeate-side pressure, sweep ratio, and membrane properties (e.g., permeance, separation factors) on MR's performance. For the AR unit, we investigate the impact of operating conditions and design parameters (e.g., W_{cat}/F_{CO} ratio, inlet H_2O/CO molar ratio, etc.). Then, we carry-out the optimization of the individual modular components and of the overall system; such an optimization entails characterizing the acceptable ranges (i.e., defining the minimums and maximums) in terms of the operating and design parameters in order to meet the selected success criteria for the process.

2. Membrane Reactor (MR)/Adsorptive Reactor (AR) Sequence

The proposed integrated IGCC system combining MR in tandem with an AR (the MR being followed by the AR) [40] is, in our opinion, the most likely one to meet the success criterion of avoiding the need to use a downstream 2-stage Selexol process. As it will be discussed below, the proposed MR-AR process is flexible, results in high CO conversions (>95%), and meets the US Department of Energy's targets for CO_2 capture (>90%) and CO_2 purity (>95%). An additional key advantage of the proposed system, when integrated within an IGCC power-plant, is that it provides a high-pressure CO_2 stream ready for sequestration.

In the proposed MR-AR process, reaction and separation take place simultaneously in the MR (employing a carbon membrane selective to H_2), and AR (using an adsorbent selective to CO_2). The AR is packed with catalyst and adsorbent pellets, while the MR contains one (for lab-scale systems) or multiple membranes, and catalyst packed in the space between the membranes and the reactor wall. During the process, the WGSR products are continuously removed from the bulk gas phase (H_2 in the MR and CO_2 in the AR), thus shifting the chemical equilibrium toward more product formation. The objective of this study is to demonstrate the feasibility of applying this product separation-enhanced reaction process in the context of an IGCC power plant, by showing that the integrated system can achieve the overall fossil energy performance goals of high

CO conversion, CO_2 capture and purity, while attaining a significant reduction in the electricity production cost as compared to baseline capture approaches.

In the analysis of the proposed integrated system, in the effort to optimize system performance, we first define the range of feasible operating conditions (for the individual system components) that allow meeting the desired process targets. For the operation of the MR, for example, for the exit of the reject side (which serves as the feed-stream for the AR) we require a minimum 1.1 H_2O/CO molar ratio (to avoid potential catalyst deactivation in the AR) and a maximum 5-10% CO_2 loss in the MR permeate side depending on the selected characteristic operating time. The AR operates under dynamic conditions, requiring adsorbent regeneration when the adsorbent is saturated. We define two characteristic times in regard to the AR's reaction/adsorption dynamic operation: (1) First, the minimum time of operation, which is defined as the time that the CO_2 breaks-through and is detected at the reactor exit, and (2) the maximum time of operation , which is the time for which the corresponding time-averaged mass flow rate of carbon exiting the AR during the entire reaction/adsorption phase (plus the carbon lost through membrane into the permeate side) up to that point reaches 10% of the constant mass flowrate of carbon entering the MR-AR sequence during the same period (this is so that we meet the US DOE target of 90% carbon capture). Defining the minimum and maximum characteristic operating times, provides the range of operating conditions within which the MR-AR system shifts between 90 - 100 % carbon capture.

The model system (depicted in Figure 1) that we study here emulates our lab-scale experimental system [40], which consists of one MR being followed by two AR's, operating alternately in reaction/adsorption and regeneration (desorption) mode due to the cyclical nature of an adsorptive reactor's operation. Indeed, continuous AR operation necessitates the use of at least two such reactors (and a greater number in a real commercial system [40]). In step one, the partially-reacted syngas gas exiting the MR (where the H_2 product is separated) is fed into the first AR, where the remaining unreacted CO is converted into CO_2 which is adsorbed. While this is occurring, the other adsorptive reactor (in which the adsorbent is now saturated with CO_2) is flushed with steam and desorption takes place producing a high-pressure stream consisting of CO_2 and H_2O. The resulting products of the system are a lower pressure humid MR permeate hydrogen stream, a high-pressure humid hydrogen stream exiting the AR during the reaction/adsorption phase, and a mixture of water and carbon dioxide exiting the AR during the desorption phase. After the adsorbent bed in the first AR saturates, the reject stream from the MR is switched to the other AR, and the regeneration of the spent adsorbent in the first AR is commenced.

An important potential advantage of the proposed MR-AR process is its reduced energy consumption, compared to the conventional process that utilizes a Dual-stage Selexol unit to separate CO_2 from the syngas exiting the WGSR. Indeed, the conventional process generates a pure CO_2 stream at approximately 1 bar, which must then be compressed to high pressures (~ 150 bar by some accounts [41]) for sequestration/utilization purposes. This compression step consumes a sizeable portion of the power produced by the power-plant. In contrast, the AR operates at much higher pressures (>20 bar), in line with the power-plant gasifier's operating pressures, and delivers a high-pressure pure CO_2 stream that requires much less energy for compression, thus attaining significant energy savings. During the desorption step, the obtained CO_2/H_2O gas mixture (at the exit of the reactor) is separated at the same pressure as the reactor exit, and the separated high-pressure H_2O is recycled for steam production in the desorption step, without the need for repeated compression.

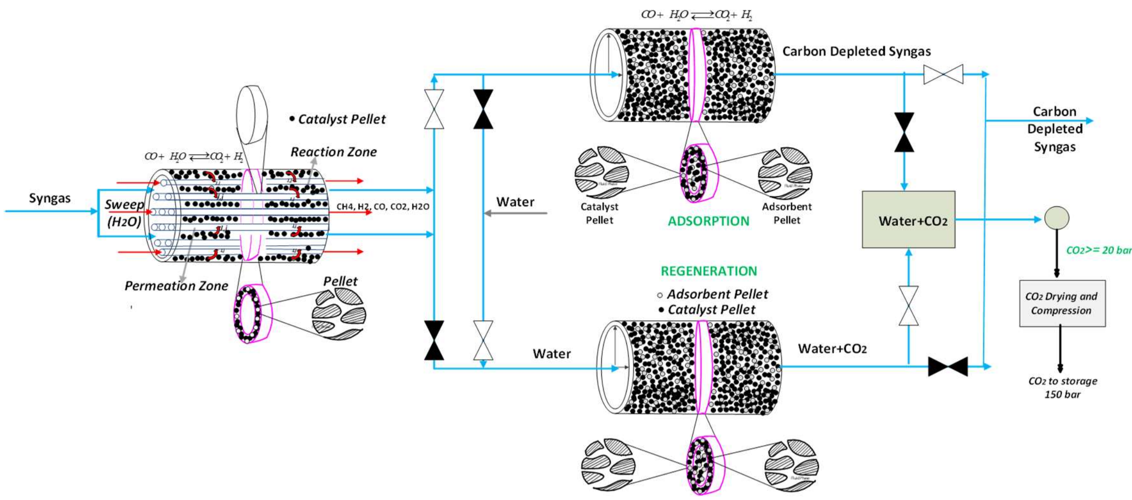

Figure 1. The proposed MR/AR Sequence Process.
(▷◁-Open Valve, ▶◀-Closed Valve)

3. Mathematical Modeling

For the study of the MR and AR we employ multiscale models. The MR consists of three domains, namely the catalyst pellet domain, the reactor domain (bulk gas phase), and permeation zone domain. The AR consists of the catalyst pellet domain, the adsorbent pellet domain and the reactor domain (bulk gas phase). At the micro level (the pellet scale) we consider all catalyst/adsorbent pellet features, including average pore size, reaction/adsorption kinetic rates, pellet material properties, and pellet shape. At the macro level (the reactor scale) we consider all the MR/AR features, such as reactor dimensions, catalyst/adsorbent packing void fraction, gas properties, etc.

An information network regarding gas pressures, temperatures, velocity, and species' concentrations in the domains is built in between the catalyst-reactor, reactor-permeation and adsorbent-reactor domains by a multiscale modeling approach. The conservation equations are simultaneously solved for each aforementioned domain by COMSOL Multiphysics®, using the finite element method. The computational fluid dynamics model employs a uniform (fine) mesh in the reactor domain, and a non-uniform mesh with 8000-unit cells in the catalyst and adsorbent pellet domains. For the radial direction of both catalyst and adsorbent pellets, we use a pre-defined mesh element distribution available in the COMSOL software, which maintains the above total number of elements in the radial direction, while ensuring that smaller unit cells are employed near the pellet surface.

For the catalyst/adsorbent pellets' domain and the reactor's domain, the mass-based conservation equations and coupled with the set of initial and boundary conditions are presented in Appendix-A. Further details about the development and numerical solution of these equations can be found in two recent papers by our Group [42-43].

4. Case Study

In a conventional IGCC plant, the WGSR is typically carried-out in a sequence of two reactors (high temperature-WGSR and low temperature-WGSR), with inter-stage cooling, to overcome both kinetic and equilibrium limitations. For pure hydrogen production, the process requires a downstream separation step to remove the CO_2 and any unreacted CO. This process is, therefore, well-suited for the application of novel intensification concepts, integrating reaction and separation into a single unit. The WGSR has also gained renewed interest recently, in both the industrial and academic sectors, due to its potential use as a main route for hydrogen production in environmentally-friendly IGCC coal power-plants, as noted above. There has been, therefore, a recent significant increase in WGSR-related studies, aiming to improve existing technologies and to potentially develop new processes that can reduce production costs.

The WGSR, Eq.(1), is exothermic, reversible, and equilibrium-limited in nature.

$$CO + H_2O \rightleftarrows CO_2 + H_2 \qquad \left(\Delta H^0_{298K} = -41.1 \;\; kJ/mol\right) \tag{1}$$

As demonstrated in Figure 2, we investigate in this paper the applicability to the IGCC process of a novel and efficient reactor configuration, which consists of a low temperature MR (LT-MR)/

followed by an AR. In the process scheme in Figure 2, the syngas produced through gasification of coal is directed into the MR-AR system that produces a hydrogen-rich stream for power generation and a pure, high-pressure CO_2 stream ready for sequestration. The hydrogen-rich stream produced by the MR-AR skid goes through a heat and power generation unit consisting of hydrogen turbines, producing energy to match the target levels defined by the performance attributes. Thus, the proposed process has the potential to become a highly efficient and ultra-compact process that produces H_2 for use in IGCC with simultaneous CO_2 capture.

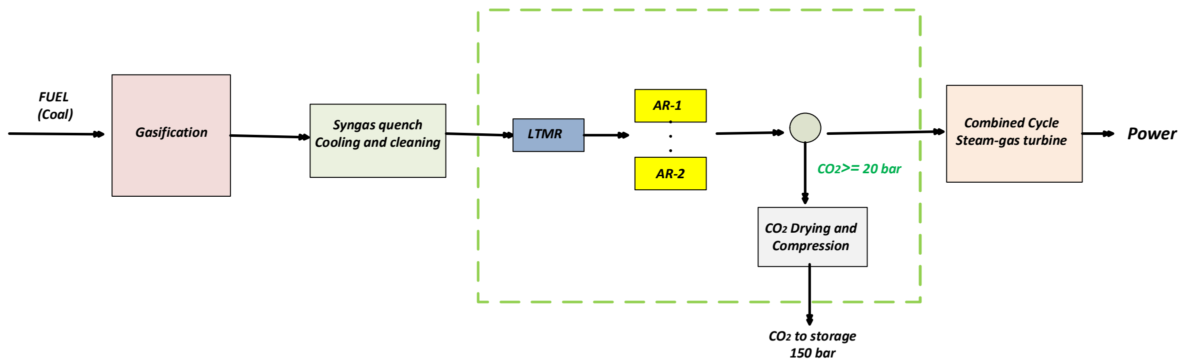

Figure 2. Simplified proposed block flow diagram of an IGCC power-plant.

4. 1. Membrane Reactor Studies:

A coal-derived syngas with composition (H_2:CO:CO_2:N_2:CH_4:H_2S:H_2O= 0.51:1.00:0.36:2.28:0.1:0.0031:1.1) is used as the feed to the MR. In the simulations, the W_{cat}/F_{CO} values in the MR were varied within a range of 20 - 95 g-cat*h/mol-CO, by changing the MR inlet flow rate, while the MR was considered to operate at a temperature of 250 ºC (simulations are carried out under adiabatic case) and a pressure of 25 bar (which are the typical conditions for the lab-scale experiments reported elsewhere [4]). In the simulations, the membrane permeances (m^3/m^2.h.bar) were taken to be: H_2=1; CO=0.0027; CO_2=0.0018; CH_4=0.0027, H_2O=0.333, which are typical of values we measure with high-quality CMS membranes prepared by our industrial collaborators in this project (Media and Process Technology, Inc.).

Species molar flow rates and molar fractions in MR:

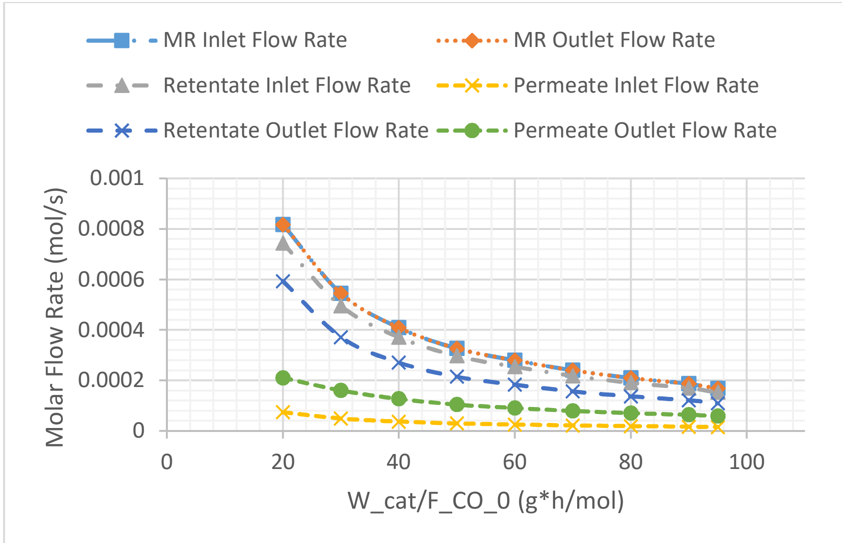

Figure 3. MR molar flow rates vs Wcat/FCO.
Sweep ratio: 0.1, permeate pressure: 4 bar

Only model simulation results are presented in Figures 3-4. Each point in these figures is obtained, following a run of the MR multi-scale model for a different value of the W_{cat}/F_{CO} ratio. Figures 3-4 show the MR outlet molar flow rates and species mole fractions as a function of W_{cat}/F_{CO}, for both reaction and permeation zones. The total inlet and outlet molar flow rates are also shown in Figure 3, for simulation consistency verification purposes. The MR inlet and outlet total molar flow rates are practically identical, thus confirming the accuracy of the simulation.

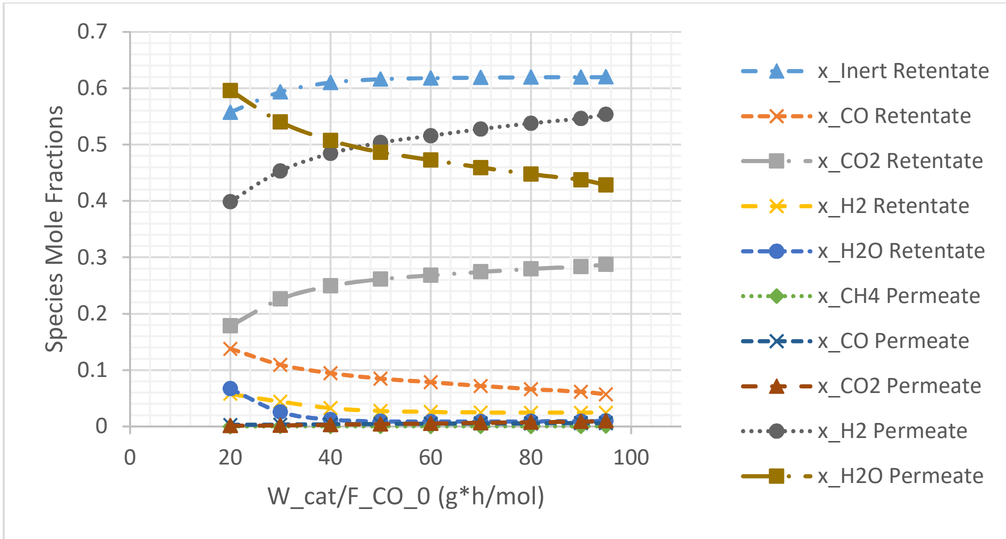

Figure 4. MR outlet species mole fractions vs. W_{cat}/F_{CO}.
Sweep ratio:0.1, permeate pressure: 4 bar

CO conversion, H_2 recovery, H_2O/CO outlet molar ratio and CO_2 lost in MR:

Simulations were carried-out, for various values of the sweep ratio and permeate-side pressure, to quantify the effect of these parameters on MR performance, and thus identify feasible operating conditions and process designs that meet the operating constraints on the MR discussed above, namely the mass of carbon lost in the permeate side being <5-10 % (depending on the characteristic operating time), and the outlet H_2O/CO ratio in the MR reject side being >1.1.

Figures 5-8 illustrate the impact of varying the sweep ratio on the CO conversion in the MR, the H_2O/CO outlet molar ratio in the reject side, the H_2 recovery (which is defined here as the molar flow rate of H_2 exiting the MR permeate side divided by the total molar flow rate of H_2 exiting the MR), and total carbon lost (ending-up) in the MR permeate side, as a function of W_{cat}/F_{CO}. As shown in Figures 5 and 7, the CO conversion and H_2 recovery are increasing functions of W_{cat}/F_{CO} for a fixed steam sweep ratio, and also increasing functions of steam sweep ratio for a fixed value of W_{cat}/F_{CO}. Indeed, Figures 5 and 7 illustrate that CO conversion (and H_2 recovery) increases from 38.5 % (67 %) at $W_{cat}/F_{CO} = 30$ and no sweep, to 85 % (95 %), at $Wcat/F_{CO} = 95$

and employing a sweep ratio = 0.3. Conversion and H_2 recovery both increase with increasing steam sweep ratio, since sweeping with steam lowers the H_2 partial pressure in the permeate side, thus enhancing H_2 transport across the membrane, and also reducing the loss of high-pressure steam (a reactant) from the reaction zone to the permeation zone. This effect is more dominant for higher W_{cat}/F_{CO} values. Another positive effect of using a sweep agent is the cooling effect provided to the reactor, as the steam in this case acts as a cooling medium. Moreover, decreasing the sweep stream temperature increases the cooling effect on the reaction zone. The downstream H_2/H_2O separation can be readily carried-out, using cooling/flashing/heating operations, thus suggesting sweeping as a promising process operation alternative.

As mentioned earlier, a goal for the proposed MR-AR process is to capture at least 90% of the carbon in its feed. Thus, a maximum 5-10 % carbon loss is allowed through the MR's membrane. Figure 8 demonstrates that the total carbon loss through the MR membrane is 0.95 %, due to the low CO_2 permeability through the membrane. Thus, this target of MR performance can be readily met.

Figure 6 shows the outlet H_2O/CO molar ratio in the MR reject side, which is an increasing function of the steam sweep ratio for fixed W_{cat}/F_{CO}, but a convex function of W_{cat}/F_{CO} for fixed steam sweep ratio, with the minimum occurring around $W_{cat}/F_{CO} = 50$, and being equal to 0.07 for no sweep and 0.15 for a sweep ratio of 0.3, while the maximum is about 0.5 and occurs at low (about 25) W_{cat}/F_{CO}. These are all lower H_2O/CO molar ratios than the target of 1.1, which is set on the basis that in the proposed MR-AR process, the MR's reject-side outlet serves as the AR's inlet, and a value of 1.1 is considered to be the safe allowable H_2O/CO molar ratio to maintain an acceptable catalyst activity in the AR. These low H_2O/CO molar ratios in the MR reject-side exit are attributable to the low steam permeate pressure of 1 bar, which leads to increased H_2O transport from the reactive zone to the permeate zone. Increasing the permeate-side pressure is, thus, a potential solution, as it is discussed below.

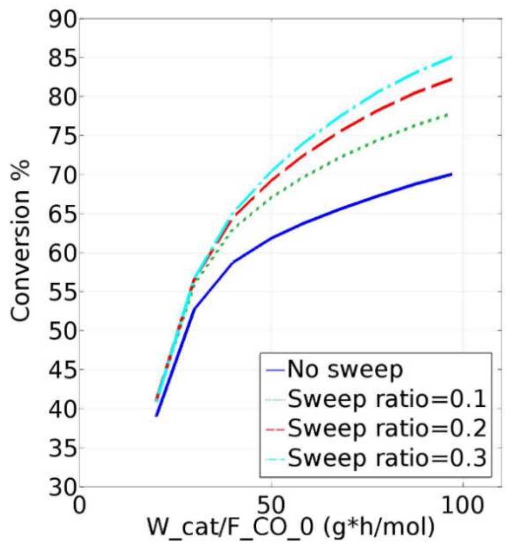

Figure 5. CO conversion vs. W_{cat}/F_{CO} .

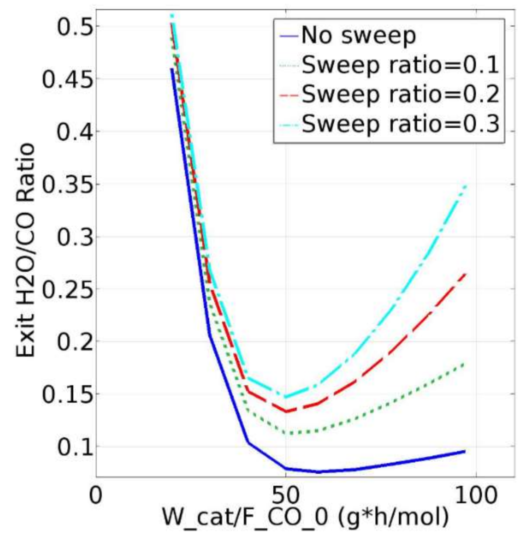

Figure 6. Exit H_2O/CO ratio vs. $Wcat/F_{CO}$. *

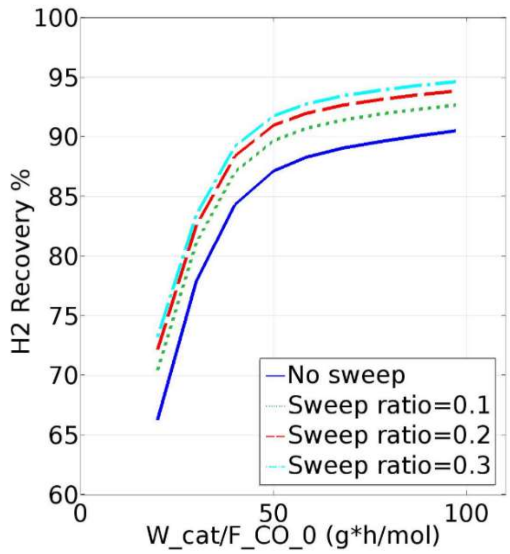

Figure 7. H_2 recovery vs. W_{cat}/F_{CO} . *

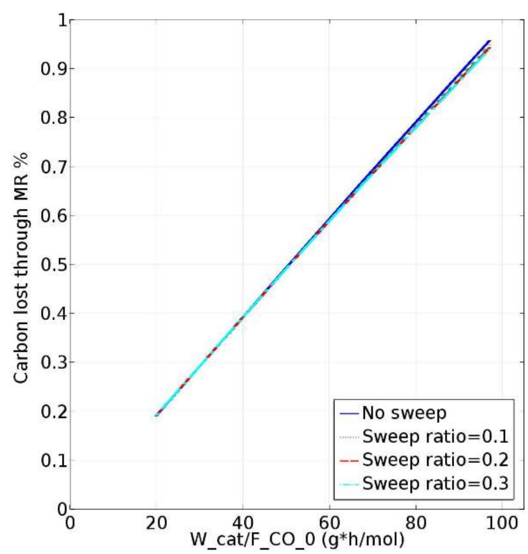

Figure 8. Carbon lost through MR vs. $Wcat/F_{CO}$. *

*Permeate inlet temperature:453 K, permeate side pressure:1 bar.

Figures 9 and 11 illustrate that at steam sweep ratio of 0.1, CO conversion (H_2 recovery) is an increasing (increasing) function of W_{cat}/F_{CO} for fixed permeate-side pressure, and an increasing (decreasing) function of permeate-side pressure, for fixed W_{cat}/F_{CO}. Indeed, Figure 9 illustrates that CO conversion increases from about 40 %, at $W_{cat}/F_{CO} =$ 20 to 77 % (84 %), at $W_{cat}/F_{CO} = 95$ and 1 bar (5 bar) permeate-side pressure. Figure 11 shows that H_2 recovery increases from about 45 % (70 %) at $Wcat/F_{CO} =$ 20 and 5 bar (1 bar) permeate-side pressure, to 60 % (93 %), at $W_{cat}/F_{CO} = 95$ and 5 bar (1 bar) permeate-side pressure.

Figure 12 demonstrates, the maximum carbon loss through the MR membrane is again 0.95 %, thus ensuring that the goal of maximum 5-10 % carbon loss in the MR continues to be satisfied at high permeate-side pressures. Figure 10 illustrates that the MR reject-side outlet H_2O/CO molar ratio is an increasing function of the permeate side pressure for fixed W_{cat}/F_{CO}, but a convex function of W_{cat}/F_{CO} for fixed permeate-side pressures, with the minimum occurring around $W_{cat}/F_{CO} = 50$ (25), and being about 0.15 (1.2) for 1 bar (5 bar) permeate-side pressure, while at $W_{cat}/F_{CO} = 95$ the MR outlet H_2O/CO molar ratio is 0.2 (2.45) for 1 bar (5 bar) permeate-side pressure. Based on the above simulation results, a permeate-side pressure of 4 bar was chosen for the integrated MR-AR system simulations to follow, as it satisfies the H_2O/CO molar ratio and CO_2 loss criteria, without undue impact on CO conversion and H_2 recovery. Another advantage of running the MR with a higher permeate-side pressure is to avoid a compression step downstream needed in using the H_2 product for power generation (e.g., in hydrogen turbines).

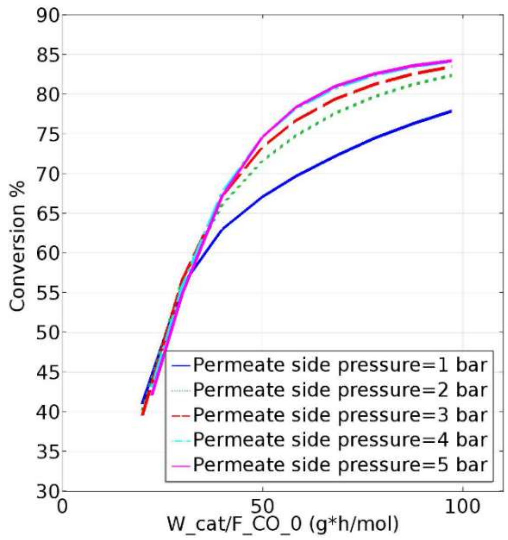

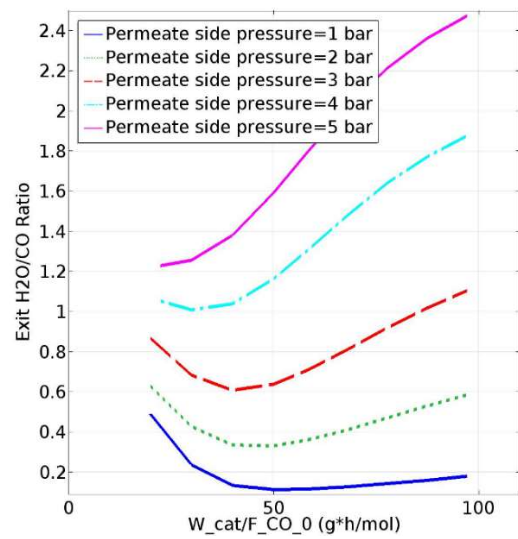

Figure 9. CO conversion vs. Wcat/F_{CO} . *

Figure 10. Exit H_2O/CO ratio vs. Wcat/F_{CO} . *

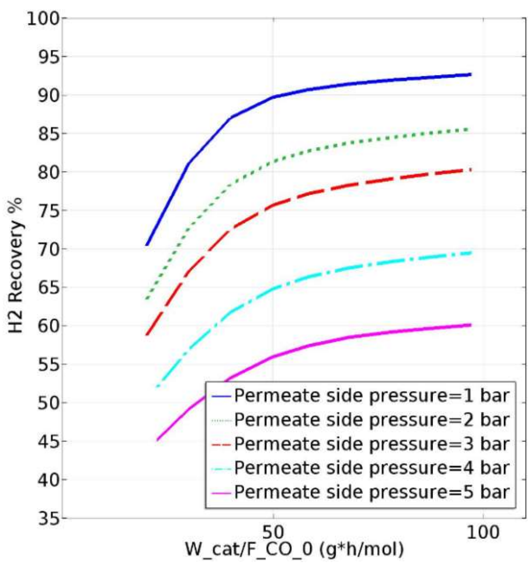

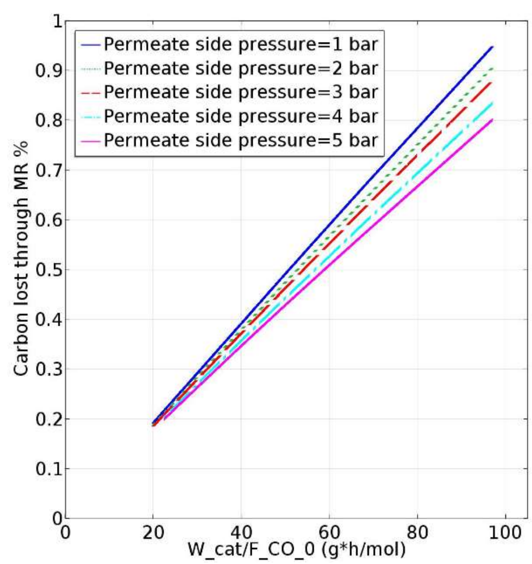

Figure 11. H_2 recovery vs. W_{cat}/F_{CO} . *

Figure 12. Carbon lost through MR vs. W_{cat}/F_{CO} . *

* Permeate inlet temperature:453 K, permeate side pressure:1 bar, sweep ratio:0.1.

Temperature profiles in the MR:

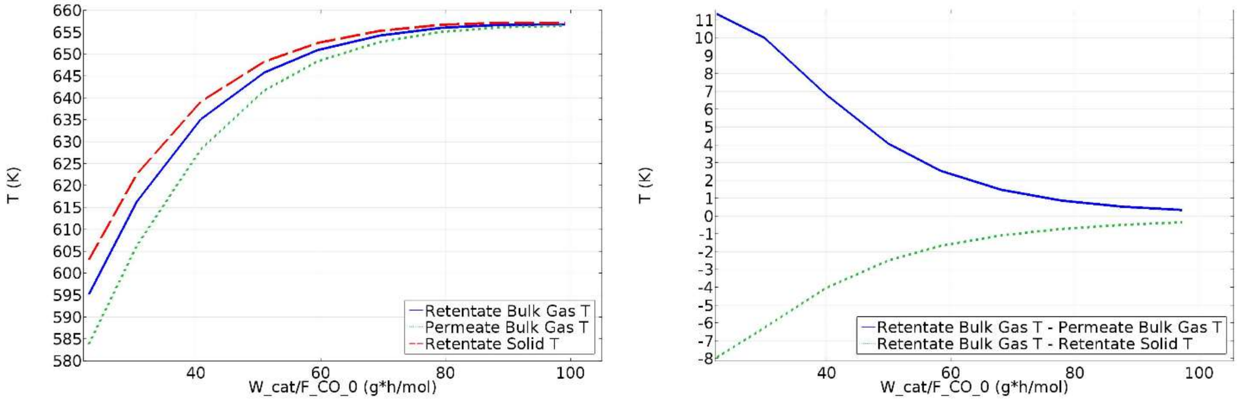

Figure 13. MR exit temperature and temperature difference profiles vs. W_{cat}/F_{CO} .
Permeate inlet temperature:453 K, permeate side pressure:1 bar, sweep ratio:0.1.

Figure 13 illustrates that the MR axial temperature profiles for the gas phase retentate and permeate sides, and for the catalyst are all increasing functions of W_{cat}/F_{CO}. Figure 13 also illustrates that the difference between the temperature of reject-side gas phase and the permeate-side gas phase (and the reject-side gas phase and catalyst-pellet temperatures) is +11 K (-8 K) for $Wcat/F_{CO}$ = 20, and +0.5 K (-0.5 K) for W_{cat}/F_{CO} = 100.

4. 2. Connecting the MR with the AR:

A number of simulations were carried-out of the integrated MR-AR system. In these simulations the steam sweep ratio in the MR was set equal to 0.1, while the permeate pressure was kept equal to 4 bar, and the W_{cat}/F_{CO} ratio was varied over a range of values which met the MR targets for the reject-side exit H_2O/CO molar ratio and the carbon loss. For each set of experimental conditions in the MR resulting in a given reject-side exit (and feed into the AR) composition, a number of AR simulations were carried out for a range of AR-W_{cat}/F_{CO} values (50-200 g-cat*h/mol-CO), and a range of W_{ad}/W_{cat} values (4-10) for the AR (W_{ad} being the weight of adsorbent utilized), with other operating conditions being a temperature of 250 ºC (simulations are carried out under wall-isothermal case), and a pressure of 25 bar, same with those employed in the reject side of the MR.

The effect of the W_{cat}/F_{CO} in the MR and of the W_{cat}/F_{CO} in the AR on the minimum/maximum AR operating times and corresponding average total conversions:

The cyclical nature of an AR's operation suggests that the time for which the AR operates in the reaction/adsorption mode is of great significance for AR process economics, flexibility and safety. It is therefore important to determine the AR's performance characteristics as defined the minimum and maximum operating times, as previously defined. Figure 14 illustrates that the minimum and maximum AR operating times are increasing functions of the W_{cat}/F_{CO} for the AR, for various AR inlet feed compositions, each of which corresponds to the reject-side exit composition in the MR for a different W_{cat}/F_{CO} ratio in the MR. The minimum (maximum) time increases from about 200 s (300 s) for $W_{cat}/F_{CO} = 80$ in the MR and $W_{cat}/F_{CO} = 50$ in the AR, to about 1500 s (2000 s) for $W_{cat}/F_{CO} = 20$ in the MR and $W_{cat}/F_{CO} = 200$ in the AR. Figure 14 also illustrates that the minimum and maximum AR operating times are decreasing functions of the W_{cat}/F_{CO} in the MR, for a fixed W_{cat}/F_{CO} in the AR. Indeed, as W_{cat}/F_{CO} in the MR increases, CO conversion at the MR exit increases, resulting in a higher CO_2 AR inlet flowrate, which then requires lower W_{cat}/F_{CO} for the AR, and thus lower minimum and maximum AR operating times.

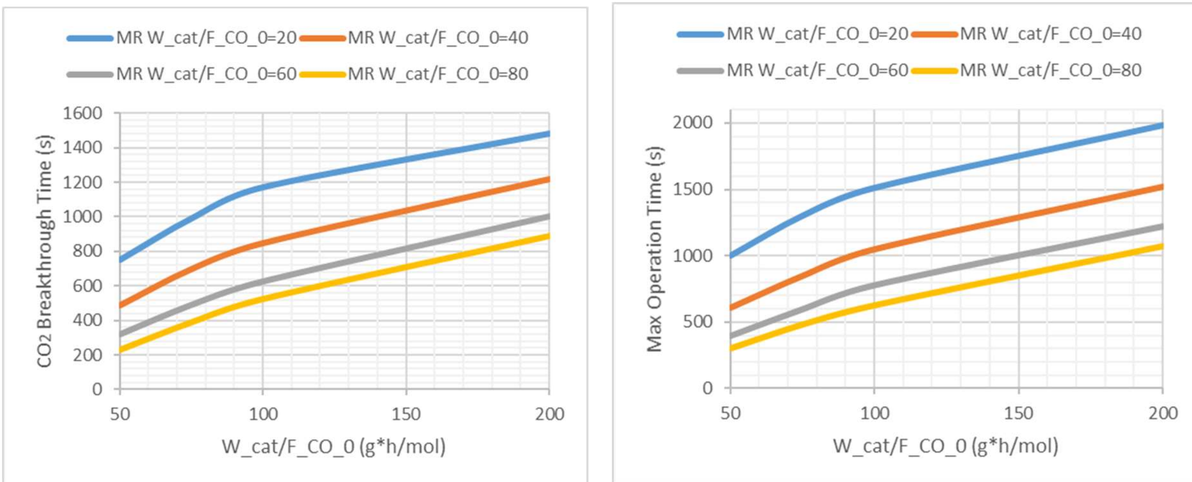

Figure 14. AR CO_2 breakthrough time[1] (Left) and AR maximum operation time[2] (Right) vs AR- W_{cat}/F_{CO} values for various MR exit compositions.
Wad/Wcat=6.

[1] The minimum time of operation, defined as the time that CO_2 is first detected at the AR exit.

[2] The maximum time of operation, defined as the time for which the time-averaged mass flowrate of carbon exiting the AR during the entire reaction/adsorption phase (including the carbon lost through the membrane) reaches 10%.

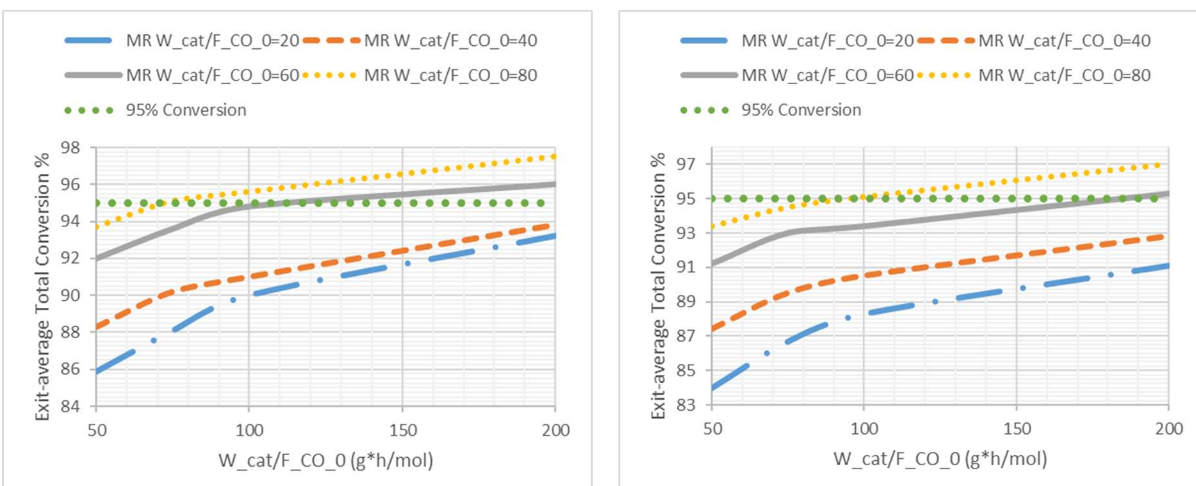

Figure 15. Exit-average total (MR+AR) CO conversion vs. AR- W_{cat}/F_{CO} values for MR exit compositions. (Left- The minimum time of operation and Right- The maximum time of operation).
W_{ad}/W_{cat} =6

Figure 15 shows the time-averaged CO conversions of the integrated MR-AR system, over both the minimum and maximum AR operating times. In Figure 15, these conversions are plotted as a function of the W_{cat}/F_{CO} for the AR for various values of the W_{cat}/F_{CO} for the MR. They are both increasing functions of W_{cat}/F_{CO} for the AR. As mentioned earlier, one of the most important success criteria for the proposed process is obtaining at least 95% total CO conversion through the combined MR/AR system. However, as can be seen in Figure 15, the total min-95% CO conversion is not acquired for all cases and AR-W_cat/F_CO_0 values. The total conversion decreases, while the value of MR-W_cat/F_CO_0 decreases. The CO conversion averaged over the minimum (maximum) operating times shown in Figure 15- Left (Figure 15-Right), values of 75, 110, 200 (100, 190, >200) AR-W_cat/F_CO_0 are needed to attain 95 % total conversion for MR-W_cat/F_CO_0 values of 80,60,50, respectively. These results suggest that 95 % conversion can be attained either running MR at higher MR-W_cat/F_CO_0 values (around 70-80) and mid-range values of AR-W_cat/F_CO_0 (around 90-100) or running MR at mid-range MR-W_cat/F_CO_0 values (around 50-60) and higher values of AR-W_cat/F_CO_0 (above 200). Increasing the inlet H_2O/CO molar ratio would be another alternative to achieve higher total conversions. Starting the MR at higher inlet H_2O/CO molar ratios may have the following effects: (1) increasing MR conversion for lower MR-W_cat/F_CO_0 values, (2) decreasing permeate side pressure (increasing H_2 recovery and CO_2 lost through membrane), (3) having higher MR outlet H_2O/CO values yields higher average toAR CO conversions, (4) increasing excess use of steam and decreasing production rate.

W_{ad}/W_{cat} effect on minimum/maximum AR operating times and corresponding average total conversions:

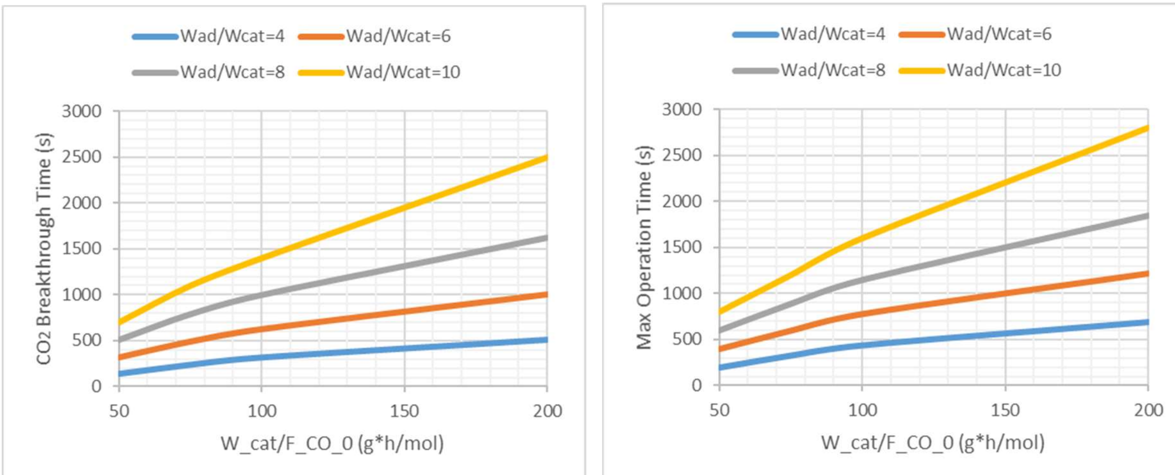

Figure 16. AR CO_2 breakthrough time (Left) and AR maximum operation time (Right) vs. AR- W_{cat}/F_{CO} values for various W_{ad}/W_{cat} values.
MR- W_{cat}/F_{CO} =60.

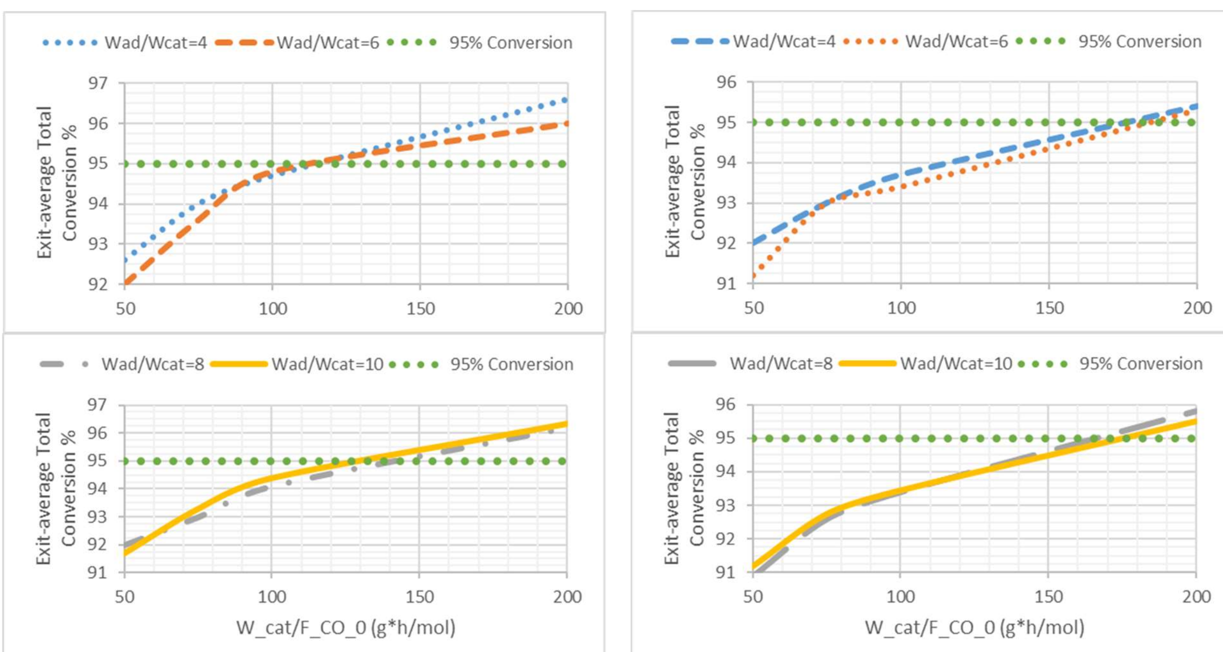

Figure 17. Exit-average total (MR+AR) CO conversion vs AR- W_{cat}/F_{CO} values for various W_{ad}/W_{cat} values.
MR-W_{cat}/F_{CO} =60.

The effect of W_{ad}/W_{cat} on the AR's minimum and maximum operating times and average total conversions is shown in Figures 16-17. As expected, CO_2 breakthrough time and maximum operating times are favored by higher W_{ad}/W_{cat} (keeping W_{cat} constant and increasing W_{ad}) ratios. Increasing the Wad/Wcat ratio from 4 to 10 increases the CO_2 breakthrough time from 500 s to 2500 s and the maximum operating time from 700 s to 2800 s. All these results suggest that the MR-AR system easily meets the >95% H_2, CO_2 purity, >90% CO_2 capture, and >95% CO conversions criteria, demanded for IGCC power plants.

The effect of the presence of the adsorbent is clear from these results, with the AR showing close to 100% conversion while the adsorbent is still fresh and effectively removes the CO_2 produced by the WGSR, thus shifting the reaction equilibrium towards the product side. Eventually, the adsorbent gets completely saturated and the AR ends operating as a PBR. As the operating pressure increases, 95 % CO conversion can still be attained, although the minimum and maximum operating times decrease significantly, since the number of CO_2 moles entering the reactor increases as the pressure increases and the inlet volumetric flow rate is kept constant. CO conversion, CO_2 breakthrough time and high-purity H_2 production are favored by higher H_2O/CO ratios. Another important phenomenon is that the pellet size is also a crucial factor for MR-AR performance, since both the reaction and the adsorption rates can be limited by intraparticle transport for larger size pellets.

Effectiveness factor evaluation in both MR and AR:

The focus of this work has been to use multi-scale modeling and simulation to explore the parameter space of this novel MR-AR process, so as to identify acceptable ranges of operating and design parameters, within which pre-defined process performance specifications can be met. In this section, the importance of local, pellet-scale behavior in determining overall process behavior is illustrated through the quantification of catalyst and adsorbent pellet effectiveness factors, as appropriate, for both the MR and AR reactors during the operation of the integrated MR-AR system.

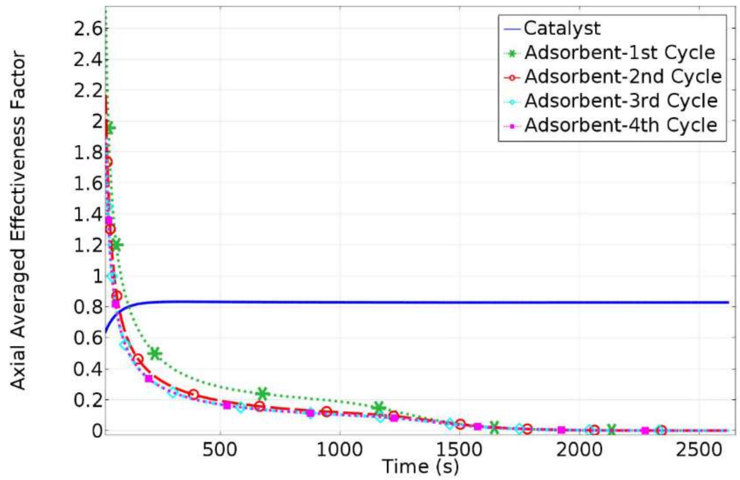

Figure 18. AR Catalyst/Adsorbent pellet axially-averaged effectiveness factors vs. time. $W_{ad}/W_{cat}=6$, AR- $W_{cat}/F_{CO}=100$

The AR axially-averaged catalyst and adsorbent effectiveness factor profiles are shown in Figure 18. The temporal effectiveness factor for the ith species is defined by Eq.(2), where the superscript ζ refers to either the catalyst or the adsorbent pellet.

$$\eta_i^{\zeta} \triangleq \frac{\iint\limits_{CS}\left(\varepsilon_{f,A}^{\zeta}\overline{N_i^{\zeta}}\right)\cdot\vec{n}\,dA^t}{\iiint\limits_{CV} M_i\varepsilon_{s,V}^{\zeta}\rho_{c/a}\,\bar{R}_i^{\zeta}\Big|_{CS}dV} = \frac{\text{the net mass flow of ith species at pellet's surface}}{\text{the volumetric mass generation rate of the same species}} \quad ; \quad i=1,\upsilon \tag{2}$$

Similarly, the length-averaged effectiveness factor is given by Eq.(3):

$$\eta_i^{ave-\zeta}(z) \triangleq \frac{\int_0^{L^r}\left[\left(\dfrac{A_c^r\varepsilon_{s,V}^r}{V^{c/a}\varepsilon_{s,V}^{c/a}}\right)\iint\limits_{CS}\left(\varepsilon_{f,A}^{\zeta}\overline{N_i^{\zeta}}\right)\cdot\vec{n}\,dA^t\right](z)\,dz}{\int_0^{L^r}\left[\left(\dfrac{A_c^r\varepsilon_{s,V}^r}{V^{\zeta}\varepsilon_{s,V}^{\zeta}}\right)\iiint\limits_{CV} M_i\varepsilon_{s,V}^{\zeta}\rho_{cat}\,\bar{R}_i^{\zeta}\Big|_{CS}dV\right](z)\,dz} \quad ; \quad i=1,\upsilon \tag{3}$$

The AR adsorbent pellet's axially-averaged effectiveness factor profiles, for each of the four consecutive AR operating cycles shown, all approach zero in about 1800 s, as adsorbent saturation is reached. During the AR desorption step, the obtained CO_2/H_2O gas mixture (at 723

K and same pressure as the adsorption step) is separated at the same pressure as the reactor exit, and the separated high-pressure H_2O is recycled in the desorption step, without the need for repeated compression. On the other hand, the AR catalyst effectiveness factor increases with time, and reaches an asymptotic value in about 200 s, as the AR begins to transition into a PBR mode of operation.

The adiabatic MR/PBR catalyst effectiveness factor axial profiles are shown in Figure 19. For the MR, the effectiveness factor decreases significantly (over 30%) along the reactor's length. For the PBR, on the other hand, the effectiveness factor decreases slightly along the reactor's length. A possible explanation for this behavior is that during adiabatic operation the reacting mixture's temperature increases along the length of both the PBR and the MR, thus accelerating the intrinsic kinetics of the WGSR more than the diffusive transport rates of the involved species, thus resulting in stronger diffusional limitations as one moves down the length of the reactor.

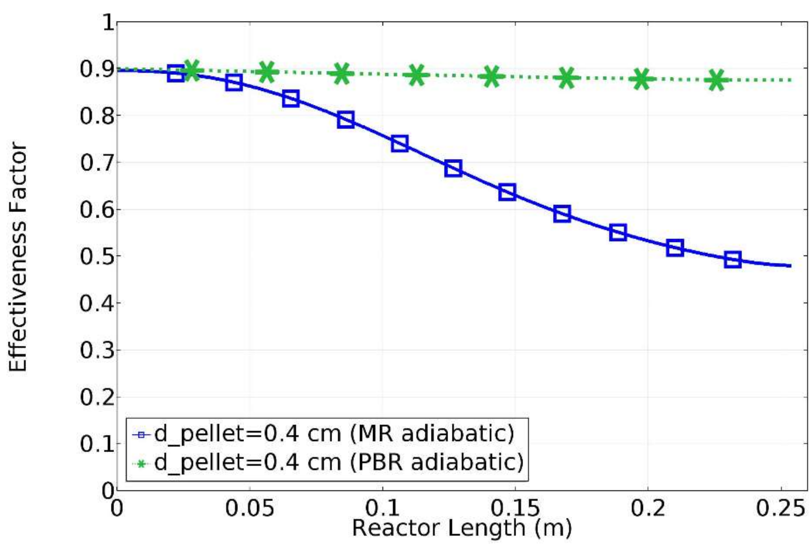

Figure 19. MR/PBR catalyst pellet effectiveness factor axial profile.
Permeate inlet temperature/pressure: 453 K/1 bar, sweep ratio:0.1, MR- W_cat/F_CO_0=60

5. Conclusions

In this study, a comprehensive, multi-scale, computational fluid dynamics (CFD) based model for the novel membrane reactor-adsorptive reactor (MR-AR) process is developed and simulated. Repeated model simulations are carried out, to study the influence of the individual units' operating and design parameters and to characterize acceptable ranges for these parameters, so as to meet predefined process performance specifications. These detailed simulation results suggest that the novel MR-AR process sequence readily fulfills carbon capture system (CCS) targets on CO conversion, H_2 purity, and CO_2 capture, and therefore represents a promising pre-combustion capture alternative for IGCC power plants.

Simulations were carried-out to quantify the effect of key MR operating conditions, such as the sweep ratio, permeate-side pressure and W_{cat}/F_{CO}. Increasing the value of W_{cat}/F_{CO} simultaneously increases CO conversion and H_2 recovery. As shown in Figures 5 and 9, for MR W_{cat}/F_{CO} values in the range of 30-95, it is possible to obtain min-38.5% (45%) and max-85% (95%) CO conversion (H_2 recovery) in the MR. Using a sweep agent and an optimally-selected permeate-side pressure can have a significant impact on the MR's behavior. The use of a sweep agent improves conversion and H_2 recovery, while increasing the permeate-side pressure reduces CO conversion, by decreasing the species' permeation rate through the membrane. A H_2O/CO molar ratio of 1.1 at the MR exit was selected in this study is the minimum such value allowable at the AR inlet, based on the need to maintain an acceptable catalyst activity in the AR. Based on the obtained simulation results, a minimum permeate-side pressure of 4 bar is required in order to satisfy at the MR exit both the H_2O/CO molar ratio, and CO_2 loss criteria. Based on these results, the MR steam sweep ratio was set to 0.1, and the MR permeate pressure was kept at 4 bar, for the remaining simulations, in which the W_{cat}/F_{CO} ratio was varied over a range of values which met the MR targets for the reject-side exit H_2O/CO molar ratio and for carbon loss in the permeate side.

The second set of simulations was carried-out to quantify the effect of key AR operating conditions, considering that the MR's reject-side exit is fed into the AR for various MR W_{cat}/F_{CO} values. The simulations show that the ratio of W_{cat}/F_{CO} has significant effect on the MR-AR system. The minimum and maximum AR operating times are increasing functions of the W_{cat}/F_{CO} for the AR, for various AR inlet feed compositions. The minimum and maximum AR operating times are decreasing functions of the W_{cat}/F_{CO} in the MR (for a fixed W_{cat}/F_{CO} in the AR). Indeed, as W_{cat}/F_{CO} in the MR increases, CO conversion at the MR exit increases, resulting in a higher CO_2 AR inlet flowrate, which then requires lower W_{cat}/F_{CO} for the AR, and thus lower minimum and maximum AR operating times. The min-95% total CO conversion is not acquired for all cases and AR W_{cat}/F_{CO} values. The total conversion decreases, while the value of MR W_{cat}/F_{CO} decreases. Based on the simulation results, 95 % conversion can be attained either by running the MR at higher MR W_{cat}/F_{CO} values (around 70-80) and the AR at mid-range values of AR W_{cat}/F_{CO} (around 90-100), or by running the MR at mid-range MR W_{cat}/F_{CO} values (around 50-60) and the AR at higher values of AR W_{cat}/F_{CO} (above 200). Increasing the inlet H_2O/CO molar ratio would be another alternative to achieve higher total conversions, while increasing W_{ad}/W_{cat} (keeping W_{cat} constant and increasing W_{ad}) ratios would lead to increases in CO_2 breakthrough, and maximum operating times.

Acknowledgements

Financial support through DOE grant DE-FE0026423 "A High Efficiency Ultra-Compact Process for Pre-Combustion CO_2 Capture" is gratefully acknowledged. Financial support from The Republic of Turkey Federal Agency for Support and Evaluation of Graduate Education within the Ministry of Education of Turkey is also gratefully acknowledged.

Nomenclature

English Symbols

$A^{\alpha}\left(m^2\ of\ domain\,\alpha\right)$ Area of the control surface of domain α

$A_c^r\left(m^2\right)$ Cross section area of the tubular reactor

$B_O\left(m^2\right)$ Viscous flow parameter of domain α

$b_i\left(Pa^{-1}\right)$ Langmuir model constant for component i

$c_{\gamma,i}^{\alpha}\left(\dfrac{mol\ of\ species\,i\ in\ phase\,\gamma\ within\,domain\,\alpha}{m^3\ of\ phase\,\gamma\ within\,domain\,\alpha}\right)$ Species' i molar density of phase γ within domain α

$c_{\gamma}^{\alpha}\left(\dfrac{mol\ of\ phase\,\gamma\ within\,domain\,\alpha}{m^3\ of\ phase\,\gamma\ within\,domain\,\alpha}\right)$ Total molar density of phase γ within domain α

$C_{P,i}^{\alpha}\left(\dfrac{J\ of\ species\,i\ in\ phase\,\gamma\ within\,domain\,\alpha}{\left(mol\cdot K\right)of\ the\ i^{th}\,component\ of\ phase\,\gamma\ within\,domain\,\alpha}\right)$ Species' i molar specific heat at constant pressure of phase f within domain α

$C_V^{\alpha}\left(\dfrac{J\ phase\,s\ within\,domain\,\alpha}{\left(mol\cdot K\right)of\ phase\,s\ within\,domain\,\alpha}\right)$ Species' i molar specific heat at constant volume of phase s within domain α

$CS^{\alpha}\left(m^2\ of\ domain\,\alpha\right)$ Control surface of domain α

$CV^{\alpha}\left(m^3\ of\ domain\,\alpha\right)$ Control volume of domain α

$D_{ij}^{\alpha}\left(\dfrac{m^2\ of\ phase\,f\ within\,of\ domain\,\alpha}{s}\right)$ Species' i and j binary diffusion coefficient of phase γ within domain α

$D_{ij}^{eff}\left(\dfrac{m^2\ of\ domain\,\alpha}{s}\right)$ Species' i and j effective binary diffusion coefficient in domain α

$D_{iK}\left(\dfrac{total\,m^2\ of\ domain\,\alpha}{s}\right)$ Species' i Knudsen diffusion coefficient in domain α

$\tilde{D}_i^r\left(\dfrac{m^2\ of\ phase\,f\ within\,domain\,r}{s}\right)$ Species' i thermal diffusion coefficient of phase f within domain r

$D_z\left(\dfrac{m^2\ of\ domain\,r}{s}\right)$ Axial dispersion coefficient in domain r

$d_p\left(m\right)$ Diameter of the pellet

$d_{pore}^p\left(m\right)$ Mean pore diameter in domain α

$d^r\left(m\right)$ Diameter of the tubular reactor

$h^{\alpha}\left(\frac{J\ from\ phase\ f\ within\ domain\ \alpha}{\left(\left(m^2\cdot K\right)of\ phase\ s\ within\ domain\ \alpha\right)\cdot s}\right)$ Interfacial heat transfer coefficient between phase f within domain α and phase s within domain α.

$\tilde{h}^{\alpha}_{\gamma,i}\left(\frac{J\ of\ phase\ \gamma\ within\ domain\ \alpha}{mol\ of\ phase\ \gamma\ within\ domain\ \alpha}\right)$ Species' i molar enthalpy of phase γ within domain α

$\lambda^{\alpha}_{\gamma}\left(\frac{J\ of\ phase\ \gamma\ within\ domain\ \alpha}{\left(\left(m\cdot K\right)of\ phase\ \gamma\ within\ domain\ \alpha\right)\cdot s}\right)$ Thermal conductivity of phase γ within domain α

$\overrightarrow{j^{\alpha}_{\gamma,i}}\left(\frac{kg\ of\ species\ i\ in\ phase\ \gamma\ within\ domain\ \alpha}{\left(m^2\ of\ phase\ \gamma\ within\ domain\ \alpha\right)\cdot s}\right)$ i^{th} species diffusion molar flux in phase γ within domain α

$\overrightarrow{J^{\alpha}_{\gamma,i}}\left(\frac{kg\ of\ species\ i\ in\ phase\ \gamma\ within\ domain\ \alpha}{\left(m^2\ of\ phase\ \gamma\ within\ domain\ \alpha\right)\cdot s}\right)$ i^{th} species combined diffusion-convection molar flux in phase γ within domain

K_{eq} Equilibrium constant of WGSR

$k_a\left(s^{-1}\right)$ Adsorption mass transfer coefficient

$L^r\left(m\right)$ Length of the tubular reactor

$M_i\left(kg\ of\ i/mol\ of\ i\right)$ i^{th} species molar mass

$m_i\left(mol/kg\right)$ Langmuir model constant for component i

$\vec{n}\left(dimensionless\right)$ Unit vector direction of the differential area dA of the CS.

$\overrightarrow{n^{\alpha}_{\gamma,i}}\left(\frac{kg\ of\ species\ i\ in\ phase\ \gamma\ within\ domain\ \alpha}{\left(m^2\ of\ phase\ \gamma\ within\ domain\ \alpha\right)\cdot s}\right)$ i^{th} species diffusion mass flux in phase γ within domain α

$\overrightarrow{N^{\alpha}_{\gamma,i}}\left(\frac{kg\ of\ species\ i\ in\ phase\ \gamma\ within\ domain\ \alpha}{\left(m^2\ of\ phase\ \gamma\ within\ domain\ \alpha\right)\cdot s}\right)$ i^{th} species combined diffusion-convection mass flux in phase γ within domain

$p^{\alpha}_{\gamma}\left(\frac{J\ of\ phase\ f\ within\ domain\ \alpha}{m^3\ of\ phase\ f\ within\ domain\ \alpha}\right)$ Pressure of phase γ within domain α

$\overrightarrow{Q^{\alpha}_{\gamma}}\left(\frac{J\ of\ phase\ \gamma\ within\ domain\ \alpha}{\left(m^2\ of\ phase\ \gamma\ within\ domain\ \alpha\right)\cdot s}\right)$ Heat flux into phase γ within domain α

$q_i\left(\dfrac{mol\ i\ on\ domain\ a}{kg\ of\ domain\ a}\right)$ Solid phase concentration of component i on domain a

$q_i^{eq}\left(\dfrac{mol\ i\ on\ domain\ a}{kg\ of\ domain\ a}\right)$ Equilibrium solid phase concentration of component i on domain a

$R_{\gamma,i}^{\alpha}\left(\dfrac{mols\ of\ species\ i\ in\ phase\ \gamma\ within\ domain\ \alpha}{\left(m^3\ of\ domain\ \alpha\right)\cdot s}\right)$ i^{th} species volumetric generation rate in phase γ within domain α

$\overline{R}_{f,i}^{\alpha}\left(\dfrac{mols\ of\ species\ i\ in\ phase\ f\ within\ domain\ p}{\left(kg\ of\ phase\ s\ within\ domain\ p\right)\cdot s}\right)$ i^{th} species phase s specific generation rate in phase f within domain α

$\tilde{R}\left(J/mol.K\right)$ Universal gas constant

R_e Reynold Number

$r\left(m\ of\ domain\ \alpha\right)$ spatial variable of domain α

$r^{\alpha}\left(m\right)$ Radius of the pellet

$T_{\gamma}^{\alpha}\left(K\right)$ Temperature of phase γ within domain α

$T^{\alpha}\left(K\right)$ Temperature of the composite phase in domain α

$T^{fur}\left(K\right)$ Temperature of the furnace

$\overrightarrow{\overrightarrow{\mathrm{T}}}_{\gamma}^{\alpha}\left(\dfrac{kg\ of\ phase\ \gamma\ within\ domain\ \alpha}{\left(m\ of\ phase\ \gamma\ within\ domain\ \alpha\right)\cdot s^2}\right)$ Viscous momentum flux tensor of phase γ within domain α

$U^{fur}\left(\dfrac{J\ transferred\ from\ domain\ r\ to\ furnace}{\left(\left(m^2\cdot K\right)of\ interphase\ contact\right)\cdot s}\right)$ Global heat transfer coefficient between the furnace and domain r

$V^{\alpha}\left(m^3\ of\ domain\ p\right)$ Total volume of domain α

$\overrightarrow{v_{\gamma}^{\alpha}}\left(m/s\right)$ Mass average velocity of the phase γ within domain α

$\overrightarrow{v_{\gamma,i}^{\alpha}}\left(m/s\right)$ i^{th} species velocity in phase γ within domain α

$w_{\gamma,i}^{\alpha}\left(\dfrac{kg\ of\ species\ i\ in\ phase\ \gamma\ within\ domain\ \alpha}{kg\ of\ phase\ \gamma\ within\ domain\ \alpha}\right)$ i^{th} species mass fraction in phase γ within domain α.

$x_{\gamma,i}^{\alpha}\left(\dfrac{mol\ of\ species\ i\ in\ phase\ \gamma\ within\ domain\ \alpha}{mol\ of\ phase\ \gamma\ within\ domain\ \alpha}\right)$ i^{th} species molar fraction in phase γ within domain α

Greek symbols:

$\varepsilon_{\gamma,V}^{\alpha}\left(\dfrac{m^3\ of\ phase\,\gamma\ within\ domain\,\alpha}{total\ m^3\ of\ domain\,\alpha}\right)$ Volumetric fraction of phase γ within domain α

$\varepsilon_{\gamma,A}^{\alpha}\left(\dfrac{m^2\ of\ phase\,\gamma\ within\ domain\,\alpha}{total\ m^2\ of\ domain\,\alpha}\right)$ Surface fraction of phase γ within domain α

$\varepsilon_{\mathrm{c-s},V}^{r}\left(\dfrac{m^3\ of\ domain\,c\ within\ domain\,r}{total\ m^3\ of\ domain\,r}\right)$ Volumetric fraction of domain c within domain r

$\varepsilon_{a-\mathrm{s},V}^{r}\left(\dfrac{m^3\ of\ domain\,a\ within\ domain\,r}{total\ m^3\ of\ domain\,r}\right)$ Volumetric fraction of domain a within domain r

$\rho_{\gamma}^{\alpha}\left(\dfrac{kg\ of\ phase\,\gamma\ within\ domain\,\alpha}{m^3\ of\ phase\,\gamma\ within\ domain\,\alpha}\right)$ Mass density of phase γ within domain α

$\rho_{\gamma,i}^{\alpha}\left(\dfrac{kg\ of\ species\,i\ in\ phase\,\gamma\ within\ domain\,\alpha}{m^3\ of\ phase\,\gamma\ within\ domain\,\alpha}\right)$ i^{th} species mass concentration in phase γ within domain α

$\tau\left(\dfrac{m\ of\ diffusion\ path\ length\ in\ phase\ f\ within\ domain\ p}{m\ of\ CV\ length\ in\ domain\ p}\right)$ Tortuosity of phase f within domain p.

$\mu_{f}^{\alpha}\left(\dfrac{kg\ of\ species\,i\ in\ phase\,\gamma\ within\ domain\,\alpha}{(m\ of\ phase\,\gamma\ within\ domain\,\alpha)\cdot s}\right)$ Viscosity of phase f within domain α

$\lambda^{\alpha}\left(J\ within\ domain\,\alpha / m^2\cdot K\cdot s\right)$ Conductivity within domain α

References

[1] Cormos, C. C. Integrated assessment of IGCC power generation technology with carbon capture and storage (CCS). Energy. 2012; 42(1):434-445.

[2] Descamps, C., Bouallou, C. and Kanniche, M. Efficiency of an integrated gasification combined cycle (IGCC) power plant including CO_2 removal. Energy.2008; 33(6): 874-881.

[3] da Cruz, F. E., & Manousiouthakis, V. I. Process intensification of reactive separator networks through the IDEAS conceptual framework. Computers & Chemical Engineering. 2017; 105: 39-55.

[4] Garshasbi, A., Chen, H., Cao, M., Karagöz, S., Ciora Jr, R. J., Liu, P. K., V. I. Manousiouthakis and Tsotsis, T. T. Membrane-based reactive separations for process intensification during power generation. Catalysis Today. 2017.

[5] Liu, Z., Grande, C. A., Li, P., Yu, J., & Rodrigues, A. E. Multi-bed vacuum pressure swing adsorption for carbon dioxide capture from flue gas. Separation and Purification Technology. 2011; 81(3): 307-317.

[6] Reynolds, S. P., Ebner, A. D., & Ritter, J. A. New pressure swing adsorption cycles for carbon dioxide sequestration. Adsorption. 2005; 11: 531-536.

[7] Harale, A., Hwang, H. T., Liu, P. K., Sahimi, M., & Tsotsis, T. T. Design aspects of the cyclic hybrid adsorbent-membrane reactor (HAMR) system for hydrogen production. Chemical Engineering Science. 2010; 65(1): 427-435.

[8] Fayyaz, B., Harale, A., Park, B.-G., Liu, P. K. T., Sahimi, M., & Tsotsis, T. T. Design aspects of hybrid Adsorbent−Membrane reactors for hydrogen production. Industrial & Engineering Chemistry Research. 2005; 44(25): 9398–9408.

[9] Lotrič, A., Sekavčnik, M., Kunze, C., & Spliethoff, H. Simulation of water-gas shift membrane reactor for integrated Gasification combined cycle plant with CO_2 capture. Strojniški vestnik – Journal of Mechanical Engineering. 2011; 57(12): 911–926.

[10] Chiappetta, G., Clarizia, G., & Drioli, E. Design of an integrated membrane system for a high level hydrogen purification. Chemical Engineering Journal. 2006; 124(1): 29-40.

[11] Chiappetta, G., Clarizia, G., & Drioli, E. Theoretical analysis of the effect of catalyst mass distribution and operation parameters on the performance of a Pd-based membrane reactor for water–gas shift reaction. Chemical Engineering Journal. 2008; 136(2), 373-382.

[12] Alfadhel, K., & Kothare, M. V. Modeling of multicomponent concentration profiles in membrane microreactors. Industrial & engineering chemistry research. 2005; 44(26): 9794-9804.

[13] Ma, D., & Lund, C. R. Assessing High-Temperature Water− Gas Shift Membrane Reactors. Industrial & engineering chemistry research. 2003; 42(4): 711-717.

[14] Lima, Fernando V., Prodromos Daoutidis, Michael Tsapatsis, and John J. Marano. Modeling and optimization of membrane reactors for carbon capture in integrated gasification combined cycle units. Industrial & Engineering Chemistry Research.2012; 51(15): 5480-5489.

[15] Georgis, Dimitrios, Fernando V. Lima, Ali Almansoori, and Prodromos Daoutidis. Thermal management of a water–gas-shift membrane reactor for high-purity hydrogen production and carbon capture. Industrial & Engineering Chemistry Research.2014; 53(18): 7461-7469.

[16] Brunetti, A., A. Caravella, G. Barbieri, and E. Drioli. Simulation study of water gas shift reaction in a membrane reactor. Journal of Membrane Science. 2007; 306 (1): 329-340.

[17] Koc, Reyyan, Nikolaos K. Kazantzis, and Yi Hua Ma. A process dynamic modeling and control framework for performance assessment of Pd/alloy-based membrane reactors used in hydrogen production. International journal of hydrogen energy. 2011; 36 (8): 4934-4951.

[18] Adrover, María E., Eduardo López, Daniel O. Borio, and Marisa N. Pedernera. Theoretical study of a membrane reactor for the water gas shift reaction under nonisothermal conditions. AIChE journal.2009; 55 (12): 3206-3213.

[19] Boutikos, Panagiotis, and Vladimiros Nikolakis. A simulation study of the effect of operating and design parameters on the performance of a water gas shift membrane reactor. Journal of Membrane Science. 2010; 350, (1): 378-386.

[20] Basile, Angelo, Giampiero Chiappetta, Silvano Tosti, and Vittorio Violante. Experimental and simulation of both Pd and Pd/Ag for a water gas shift membrane reactor. Separation and purification technology. 2001; 25 (1): 549-571.

[21] Basile, Angelo, Luca Paturzo, and Fausto Gallucci. Co-current and counter-current modes for water gas shift membrane reactor. Catalysis today. 2003; 82 (1): 275-281.

[22] Mendes, Diogo, Sandra Sá, Silvano Tosti, José M. Sousa, Luis M. Madeira, and Adélio Mendes. Experimental and modeling studies on the low-temperature water-gas shift reaction in a dense Pd–Ag packed-bed membrane reactor. Chemical engineering science. 2011; 66 (11): 2356-2367.

[23] Chein, R. Y., Y. C. Chen, and J. N. Chung. Sweep gas flow effect on membrane reactor performance for hydrogen production from high-temperature water-gas shift reaction. Journal of Membrane Science. 2015; 475: 193-203.

[24] Dong, Xueliang, Haibing Wang, Zebao Rui, and Y. S. Lin.Tubular dual-layer MFI zeolite membrane reactor for hydrogen production via the WGS reaction: Experimental and modeling studies. Chemical Engineering Journal. 2015; 268: 219-229.

[25] Castro-Dominguez, Bernardo, Ivan P. Mardilovich, Rui Ma, Nikolaos K. Kazantzis, Anthony G. Dixon, and Yi Hua Ma. Performance of a pilot-scale multitube membrane module under coal-derived syngas for hydrogen production and separation. Journal of Membrane Science. 2017; 523: 515-523.

[26] Wang, Y., Chao, Z., Chen, D., & Jakobsen, H. A. SE-SMR process performance in CFB reactors: Simulation of the CO2 adsorption/desorption processes with CaO based sorbents. International Journal of Greenhouse Gas Control. 2011; 5(3): 489-497.

[27] Reijers, H. T. J., Boon, J., Elzinga, G. D., Cobden, P. D., Haije, W. G., & van den Brink, R. W. Modeling study of the sorption-enhanced reaction process for CO_2 capture. I. Model development and validation. Industrial & Engineering Chemistry Research. 2009; 48(15): 6966-6974.

[28] Reijers, H. T. J., Boon, J., Elzinga, G. D., Cobden, P. D., Haije, W. G., & Brink, R. W. V. D. Modeling study of the sorption-enhanced reaction process for CO_2 capture. II. Application to steam-methane reforming. Industrial & Engineering Chemistry Research. 2009; 48(15): 6975-6982.

[29] Halabi, M. H., De Croon, M. H. J. M., Van Der Schaaf, J., Cobden, P. D., & Schouten, J. C. Reactor modeling of sorption-enhanced autothermal reforming of methane. Part I: Performance study of hydrotalcite and lithium zirconate-based processes. Chemical engineering journal. 2011; 168(2): 872-882.

[30] Halabi, M. H., De Croon, M. H. J. M., Van der Schaaf, J., Cobden, P. D., & Schouten, J. C. Reactor modeling of sorption-enhanced autothermal reforming of methane. Part II: effect of operational parameters. Chemical engineering journal. 2011; 168(2): 883-888.

[31] Ding, Y., & Alpay, E. Adsorption-enhanced steam–methane reforming. Chemical Engineering Science. 2000; 55(18): 3929-3940.

[32] Xiu, G., Li, P., & Rodrigues, A. E. Adsorption-enhanced steam-methane reforming with intraparticle-diffusion limitations. Chemical Engineering Journal. 2003; 95(1-3): 83-93.

[33] Chanburanasiri, N., Ribeiro, A. M., Rodrigues, A. E., Laosiripojana, N., & Assabumrungrat, S. Simulation of methane steam reforming enhanced by in situ CO2 sorption using K_2CO_3-promoted hydrotalcites for H_2 production. Energy & Fuels. 2013; 27(8): 4457-4470.

[34] Jakobsen, H. A. Chemical reactor modeling. Multiphase Reactive Flows, Berlin, Germany: Springer-Verlag, 2008.

[35] Whitaker, S. Flow in porous media I: A theoretical derivation of Darcy's law. Transport in porous media. 1986; 1(1): 3-25.

[36] Joshi, S. Y., Harold, M. P., & Balakotaiah, V. On the use of internal mass transfer coefficients in modeling of diffusion and reaction in catalytic monoliths. Chemical Engineering Science. 2009; 64(23): 4976-4991.

[37] Miller, C. T., Christakos, G., Imhoff, P. T., McBride, J. F., Pedit, J. A., & Trangenstein, J. A. Multiphase flow and transport modeling in heterogeneous porous media: challenges and approaches. Advances in Water Resources. 1998; 21(2): 77-120.

[38] Whitaker, S. Simultaneous heat, mass, and momentum transfer in porous media: a theory of drying. Advances in heat transfer. 1977; 13: 119-203.

[39] Bey, O., & Eigenberger, G. Fluid flow through catalyst filled tubes. Chemical Engineering Science. 1997; 52(8): 1365-1376.

[40] Chen, H., Cao, M., Zhao, L., Ciora Jr, R. J., Liu, P. K., Manousiouthakis, V. I., & Tsotsis, T. T. Experimental Study of an Intensified Water–Gas Shift Reaction Process Using a Membrane Reactor/Adsorptive Reactor Sequence. Industrial & Engineering Chemistry Research. 2018; 57(41): 13650-13660.

[41] Mukherjee, S., Kumar, P., Yang, A. and Fennell, P. Energy and exergy analysis of chemical looping combustion technology and comparison with pre-combustion and oxy-fuel combustion technologies for CO2 capture. Journal of environmental chemical engineering. 2015; 3(3): 2104-2114.

[42] Karagöz, S., da Cruz, F. E., Tsotsis, T. T., & Manousiouthakis, V. I. Multi-scale membrane reactor (MR) modeling and simulation for the water gas shift reaction. Chemical Engineering and Processing-Process Intensification. 2018; 133: 245-262.

[43] Karagöz, S., Chen, H., Cao, M., Tsotsis, T. T, & Manousiouthakis, V. I. Energy intensification of H_2 generation and CO_2 capture/utilization by a Novel Adsorptive Reactor (AR) Process. AIChE Journal-Submitted. 2018